Available online at www.sciencedirect.com
SCIENCE DIRECT®
Optics Communications 232 (2004) 179–199
OPTICS COMMUNICATIONS
www.elsevier.com/locate/optcom

Performance analysis of ultrafast all-optical Boolean XOR gate using semiconductor optical amplifier-based Mach–Zehnder Interferometer

T. Houbavlis [a], K.E. Zoiros [b,*], G. Kanellos [a], C. Tsekrekos [a]

[a] School of Engineering, Department of Electrical and Computer Engineering, Photonics Communications Research Laboratory, National Technical University of Athens, 9 Iroon Polytechniou Street, GR 157 73 Athens, Greece
[b] School of Engineering, Department of Electrical and Computer Engineering, Laboratory of Telecommunications Systems, Democritus University of Thrace, 12 Vas. Sofias Street, GR 671 00 Xanthi, Greece

Received 9 September 2003; accepted 22 December 2003

Abstract

An all-optical Boolean XOR gate implemented with a SOA-based Mach–Zehnder Interferometer (SOA-MZI) is numerically simulated at 10 and 40 Gb/s to extract simple design rules. If the control and clock energies are properly selected so that the SOAs are heavily saturated and at the same time the switched-out pulses are not distorted, the metrics that define the quality of switching can be optimized for high gate performance at 10 Gb/s. However, the operation at 40 Gb/s is limited by the SOAs gain recovery time that results in strong pattern dependence of the output pulses and so the extension to this rate requires the deployment of gain recovery reduction techniques in bulk and quantum-well SOAs or alternatively the exploitation of other technologically advanced optical devices, such as quantum-dot SOAs.

Keywords: All-optical Boolean XOR logic; All-optical signal processing; All-optical switching; Semiconductor optical amplifier (SOA); SOA-based Mach–Zehnder Interferometer (SOA-MZI); Optical time division multiplexing (OTDM) networks

1. Introduction

High-capacity optical communication systems are evolving rapidly to satisfy the numerous and diverse needs of the new broadband network environment, which is characterized by the rapid convergence of telecommunications and informatics and the massive use of Internet and multimedia applications. All-optical signal processing such as demultiplexing, wavelength conversion, regeneration and Boolean logic will play a critical role in the development of these terabit transmission systems [1]. The inherent capability of this technology to handle a single ultra-high speed data channel exclusively in the optical domain without

* Corresponding author. Tel.: +30-25410-79-975; fax: +30-25410-79-595.
E-mail address: kzoiros@ee.duth.gr (K.E. Zoiros).

0030-4018/$ - see front matter © 2003 Elsevier B.V. All rights reserved.
doi:10.1016/j.optcom.2003.12.062

optoelectrical conversions can significantly improve the performance of the photonic systems in terms of flexibility, scalability, wavelength management simplification, optical components minimization and cost reduction. In order to realize the all-optical signal processing functions, various interferometric all-optical switches have been investigated that exploit the ultrafast nonlinear properties of semiconductor optical amplifiers (SOAs) [2]. Among switching configurations, such as the Sagnac/Terahertz Optical Asymmetric Demultiplexer (TOAD) [3] and the Ultrafast Nonlinear Interferometer (UNI) [4], the SOA-based Mach–Zehnder Interferometer (SOA-MZI) is the most promising candidate due to its attractive features of low energy requirement, short latency, high stability and compactness that enables integration and possible mass production [5]. Using this type of switch, a set of processing operations ranging from demultiplexing [6] to regeneration [7] and wavelength conversion [8] to optical sampling [9] and optical flip-flops [10] has been demonstrated. Particular attention has also attracted the all-optical XOR gate, which is a key technology to implement primary systems for binary address and header recognition, binary addition and counting, pattern matching, decision and comparison, generation of pseudorandom binary sequences, encryption and coding. This gate has been demonstrated at 10 Gb/s [11–13], 20 Gb/s [14] and 40 Gb/s [15] using SOA-MZI differential schemes that have been deployed to overcome the strong speed limitations imposed by the SOA's slow recovery time. However, the improvement in performance is achieved at the cost of increased complexity (for example, a high degree of synchronization accuracy is required) and the problem of amplitude modulation due to pattern effects is not eliminated. It would be useful thus to investigate in an extensive and systematic manner how the simple, standard SOA-MZI architecture can be exploited as an XOR gate at high rates from 10 to 40 Gb/s, essentially extending the range of its Boolean applications which has been limited so far to the AND operation [16–18]. This paper aims to achieve this goal through numerical simulation in terms of the gate's critical parameters and to provide simple design rules for the improvement of its performance. The obtained results will be very useful in the optimum design of semiconductor gates, improve the knowledge in the field and significantly contribute to the thorough analysis of other more complex all-optical circuits that employ the XOR gate as the basic building block, particularly in feedback applications, and that cannot be sufficiently simulated by the commercially available photonic software tools.

2. Operation principle and model formulation

The optical XOR gate in our study consists of a symmetrical MZI with two SOAs placed in the upper and lower arms of the interferometer, as shown in Fig. 1. In order to perform the Boolean XOR operation, two optical control beams A and B that may take a logical '0' and '1' enter the upper and lower arms of the MZI via two Wavelength Selective Couplers (WSC). A clock stream held continuously to a logical '1' is inserted in the MZI and split into two equal parts via the input 3 dB coupler. In case that both A and B are '1' or '0', the MZI is balanced and ideally the entire clock exits at the reflection port (R). However, when either A or B is '1', the cross-phase modulation (XPM) between the control and clock pulses inside the SOAs creates a differential phase shift between the two clock components, which when it is made equal to π radians best switching is achieved at the transmission port (T). Note that in this configuration no filter is required at the output to reject the control signal since the control and clock pulses counterpropagate through the arms of the MZI.

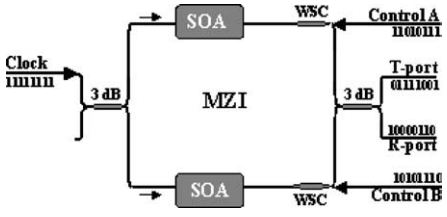

Fig. 1. Configuration of all-optical XOR gate using SOA-MZI. WSC: Wavelength Selective Coupler.

To simulate the performance of the SOA-MZI XOR gate, the comprehensive model of Tang and Shore [19] that successfully describes the propagation and amplification of strong picosecond optical pulses through a SOA is utilized but appropriately altered so that the contribution of the clock and control pulses on the SOAs properties is equal in a way similar to the model in [20]. The goal of this approach was to investigate the effect of the clock's dynamic range on the SOAs saturation and consequently on the performance of the gate. The effect of the amplified spontaneous emission (ASE) has not been taken into account in our simulation because its influence on the gate's performance is negligible. This is due to the relatively high power levels of both control and clock signals that deeply saturate the SOAs and also because the SOA-MZI performance depends on ASE when long SOAs (>1500 μm) are used [16,21], which is not our case. We have assumed also that the clock and control signals enter synchronized the two SOAs, which are identical, and that the initial phase of the clock pulses in each arm is zero. The ultrafast dynamics of the SOAs are governed by carrier heating (CH), spectral hole burning (SHB), two-photon absorption (TPA) and ultrafast nonlinear refraction (UNR) processes [22]. However, the influence of the two latter effects becomes significant for pulses of the order of hundreds of femtoseconds and so they can be neglected because we are interested in the dynamics of pulses that are few picoseconds or more wide. On the other hand, CH and SHB are the intraband processes that provide the dominant contribution to gain saturation for the case of pulses shorter than 10 ps and must be thus taken into account. Furthermore, the gain as well as the loss are assumed to be wavelength independent since we are not interested in investigating the influence of this parameter on the performance of the gate and because this would require the use of a second-order polynomial approximation of the gain spectrum [23], inevitably complicating our model. Within this frame, the central frequency of the control pulses is assumed to be located at the peak of the SOAs gain spectrum and the frequency detuning between the control and clock signals to be higher than 1 THz so that the formed temporal gratings do not play an important role in determining the responses of the SOAs and can be omitted [23]. An additional approximation is that the group-velocity dispersion is neglected, which is satisfied for picosecond pulsewidths [24].

The SOA is treated as a traveling wave amplifier with null facet reflectivities and it is assumed, for ease of analysis, that it behaves as an isotropic device. This simplification allows to treat the susceptibility tensor, $\tilde{\chi}$, as a scalar.

The equations that describe the carrier dynamics in the SOA are

$$\frac{\partial N}{\partial t} = \frac{I}{qV} - \frac{N}{\tau_{\text{car}}} - \frac{1}{\Gamma\sigma\hbar\omega}\frac{G|\vec{E}|^2}{1+\varepsilon|\vec{E}|^2}, \tag{1}$$

$$\chi = \frac{-\bar{n}c}{\omega\Gamma} G\left(\frac{L}{1+\varepsilon|\vec{E}|^2} + \alpha_N\right), \tag{2}$$

where N is the carrier density, I the injection current, q the electron charge, $V = wdL$ the active region volume, with w, d and L being the width, depth and length of the active region, respectively, τ_{car} the carrier lifetime, Γ the confinement factor, σ the mode cross-section ($= wd/\Gamma$), $\hbar = h/2\pi$, where h is Planck's constant, ω the frequency of the electromagnetic radiation, $\vec{E}$ the total electric field, $\bar{n}$ the effective mode index, c the speed of light in vacuum and α_N the traditional linewidth enhancement factor. G stands for the modal gain that can be assumed to vary linearly with N as

$$G = \Gamma\alpha_{\text{N}}(N - N_{\text{tr}}), \tag{3}$$

where α_{N} is the differential gain and N_{tr} the carrier density at transparency. The parameter $\varepsilon = \varepsilon_{\text{SHB}} + \varepsilon_{\text{CH}}$ includes the nonlinear gain compression effects produced by SHB and CH.

Noting from (3) that $N = G/\Gamma\alpha_{\text{N}} + N_{\text{tr}}$, substituting in (1) and doing some algebraic manipulations, the following equation for the gain can be obtained

$$\frac{\partial G_j}{\partial t} = \frac{G_{\text{ss}} - G_j}{\tau_{\text{car}}} - \frac{G_j|\vec{E}|^2}{E_{\text{sat}}(1+\varepsilon|\vec{E}|^2)}, \tag{4}$$

where the subscript $j =$ "s" or "c" has been appended to G to denote either the gain of the clock or control signal, $G_{\text{ss}} = \Gamma\alpha_N N_{\text{tr}}(I/I_{\text{tr}} - 1)$ is the small signal gain, $I_{\text{tr}} = qVN_{\text{tr}}/\tau_{\text{car}}$ is the injected

current required for transparency and $E_{sat} = \hbar\omega\sigma/\alpha_N$ is the saturation energy of the SOA.

The wave equation for the electromagnetic field in the SOA is governed by

$$\nabla^2 E_j - \frac{1}{c^2}(n_b^2 + \chi)\frac{\partial^2 E_j}{\partial t^2} = 0, \tag{5}$$

where n_b is the background refractive index. By a procedure similar to that used in [25], an equation describing the propagation of the optical pulse in the SOA can be obtained from (2) and (5)

$$\frac{\partial A_j(z,t)}{\partial z} + \frac{1}{u_g}\frac{\partial A_j(z,t)}{\partial t} = \frac{1}{2}\frac{G_j A_j(z,t)}{1+\varepsilon|\vec{E}|^2} - \frac{j}{2}G_j A_j(z,t)\alpha_N - \frac{1}{2}\alpha_{int}A_j(z,t), \tag{6}$$

where u_g is the group velocity and α_{int} are the linear internal losses.

In (4) and (6) the squared modulus of the total electrical field $|\vec{E}|^2$ may be written as

$$\vec{E}\cdot\vec{E}^* = \sum_j E_j E_j^* = |A_s|^2 + |A_c|^2, \tag{7}$$

where $*$ stands for complex conjugate.

Transforming to the retarded reference frame, $t \to t - z/u_g$, separating A into an amplitude and phase

$$A_j(z,t) = \sqrt{P_j(z,t)}\exp[i(\varphi_j(z,t))], \tag{8}$$

where $P_j(z,t)$ and $\varphi_j(z,t)$ are the transmitted optical power and nonlinear phase shift, respectively, and using (7), the following final set of equations can be obtained from (4) and (6)

$$\frac{\partial P_c(z,t)}{\partial z} = \frac{G_c(z,t)}{1+\varepsilon[P_c(z,t)+P_s(z,t)]}P_c(z,t) - \alpha_{int}P_c(z,t), \tag{9}$$

$$\frac{\partial \varphi_c(z,t)}{\partial z} = -\frac{1}{2}\alpha_N G_c(z,t), \tag{10}$$

$$\frac{\partial G_c(z,t)}{\partial t} = \frac{G_{ss} - G_c(z,t)}{\tau_{car}} - \frac{1}{E_{sat}} \times \frac{G_c(z,t)[P_c(z,t)+P_s(z,t)]}{1+\varepsilon[P_c(z,t)+P_s(z,t)]}, \tag{11}$$

$$\frac{\partial P_s(z,t)}{\partial z} = \frac{G_s(z,t)}{1+\varepsilon[P_c(z,t)+P_s(z,t)]}P_s(z,t) - \alpha_{int}P_s(z,t), \tag{12}$$

$$\frac{\partial \varphi_s(z,t)}{\partial z} = -\frac{1}{2}\alpha_N G_s(z,t), \tag{13}$$

$$\frac{\partial G_s(z,t)}{\partial t} = \frac{G_{ss} - G_s(z,t)}{\tau_{car}} - \frac{1}{E_{sat}} \times \frac{G_s(z,t)[P_c(z,t)+P_s(z,t)]}{1+\varepsilon[P_c(z,t)+P_s(z,t)]}, \tag{14}$$

where the subscript j has been replaced by "s" or "c". In the above equations the local time takes values between 0 and $T = N \cdot T_{per}$, with T_{per} being the pulse period, N is the number of bits the pulse sequence consists of and z is the space variable with values between 0 and the SOA length, L. Note that the sum $P_c + P_s$ essentially implies that not only the control but also the clock pulses have sufficient energy to modify the SOAs optical properties, in contrast to the usual approach that the gain saturation is caused only by the intense control pulses [23].

In order to solve the above set of equations, the following initially conditions are required:

(i) $G_c(z,0) = G_{ss}$ and $G_s(z,0) = G_{ss}$, $\forall z \in [0,L]$

(ii) $P_c(0,t) = \mathrm{Seq}[t(\mathrm{div})T_{per}]C_c\, e^{-\left(\frac{t-[t(\mathrm{div})T_{per}]T_{per}-n_t}{t_{0c}}\right)^2}$ and

$P_s(0,t) = C_s e^{-\left(\frac{t-[t(\mathrm{div})T_{per}]T_{per}-n_t}{t_{0s}}\right)^2}$, $\forall t \in [0, N\cdot T_{per}]$.

The first condition implies that the leading edge of the first pulse ($t = 0$) of the sequence inserted in the SOAs experiences an unsaturated small signal gain since the SOAs have not been brought to saturation yet. The second condition expresses the fact that the signal arriving at the input SOA facets ($z = 0$) is a sequence of Gaussian-shaped pulses of width t_{0c} and t_{0s} for the control and clock, respectively. This pulsewidth, t_0, is related to the full width at half maximum, T_{FWHM}, with the relationship $T_{FWHM} = 2t_0\sqrt{\ln 2}$ [25]. The constants C_c and C_s are the peak power values of the control and clock pulses, respectively. Seq $[\cdot]$ is a single-dimension array that contains N elements of '0' and '1', i.e. the bits of the control sequence. A similar term is not used for the clock sequence since it comprises only of consecutive '1'. The term $t(\mathrm{div})T_{per}$ denotes the integer part of the ratio $\frac{t}{T_{per}}$

and the constant n_t is used so that the energy of the first pulse of each sequence is contained entirely in the interval $[0, N \cdot T_{\text{per}}]$.

The set of Eqs. (9)–(14) with the defined initial conditions cannot be solved in closed-form but only numerically. For this purpose, the optical pulses and the SOAs have been divided in many small segments in time and distance, respectively and solutions have been obtained stepwise both in time and space for the temporal gain and phase changes experienced by the clock pulses in the two arms of the interferometer. These are required to calculate the characteristics of the switched-out clock pulses at the transmission and reflection port of the interferometer, expressed by the equations [26]

$$T(t) = 1/4\{G_1(t) + G_2(t) - 2\sqrt{G_1(t)G_2(t)} \times \cos[\varphi_1(t) - \varphi_2(t)]\}, \quad (15)$$

$$R(t) = 1/4\{G_1(t) + G_2(t) + 2\sqrt{G_1(t)G_2(t)} \times \cos[\varphi_1(t) - \varphi_2(t)]\}, \quad (16)$$

where $T(t)$ and $R(t)$ are the transmission and reflection functions and $G_1(t)$, $G_2(t)$, $\varphi_1(t)$, $\varphi_2(t)$ are the time-dependent power gains and phases experienced by the clock pulses in the upper and lower interferometer arms, respectively. The power gain equals $\frac{P_s(L,t)}{P_s(0,t)}$ and the difference between the phases of the clock pulses in the two arms of the interferometer is

$$\varphi_1(t) - \varphi_2(t) = \alpha_N \frac{1}{2} \ln\left(\frac{G_1(t)}{G_2(t)}\right), \quad (17)$$

where α_N is the linewidth enhancement factor.

3. Results and discussion

Table 1 lists the values of the SOA parameters used in the simulation which are representative of bulk InGaAsP SOAs operating in the 1550 nm spectral region and are in accordance with theoretical and experimental data provided for this type of SOAs in literature [20,21]. The value of the gain coefficient varies since it depends on the driving injection current and can be considered as a "free" parameter. In the following, the small signal gain coefficient takes three values, namely 5132, 5792 and 6636 m^{-1}, which correspond to small signal power gain 20.4, 24.7 and 30.2 dB, respectively. The duty cycle was held constant to 7/100 with the pulse FWHM being 7 and 1.75 ps at 10 and 40 Gb/s, respectively.

In order to assess the performance of the gate at 10 and 40 Gb/s, we defined and calculated

Table 1
SOA parameters used in the calculations

Parameter	Symbol	Value
Length of active region	L	1500 μm
Depth of active region	d	0.250 μm
Width of active region	w	2 μm
Confinement factor	Γ	0.48
Mode cross-section	σ	1042×10^{-15} m^2
Group refractive index	n_g	3.62
Small signal gain	G_{ss}	5132, 5792 and 6636 m^{-1} corresponding to small signal power gain 20.4, 24.7 and 30.2 dB, respectively
Differential gain at $\lambda_{max} = 1550$ nm	α_N	3.3×10^{-20} m^2
Linewidth enhancement factor	α_N	6
Carrier density at transparency	N_{tr}	1.0×10^{24} m^{-3}
Injection current	I	0.80–0.85 A
Transparency current	I_{tr}	0.6 A
Nonlinear gain compression factor	$\varepsilon = \varepsilon_{SHB} + \varepsilon_{CH}$	0.2 W^{-1}
Carrier lifetime	τ_{car}	200 ps
Saturation energy	E_{sat}	1 pJ
Linear internal losses	α_{int}	2000 m^{-1}

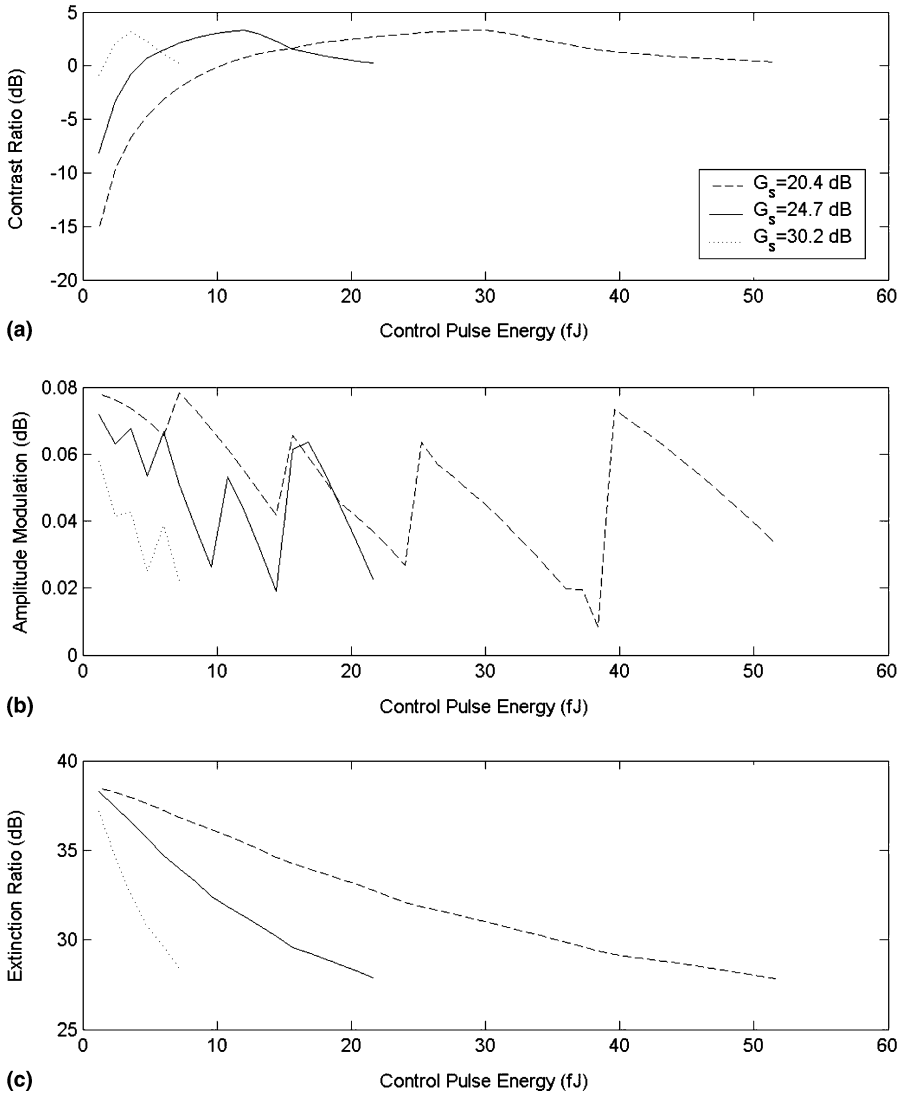

Fig. 2. Calculated metrics at 10 Gb/s for low SOA saturation, (a) contrast ratio, (b) amplitude modulation and (c) extinction ratio.

metrics characterizing the quality of switching such as the contrast ratio (CR), the amplitude modulation (AM) and the extinction ratio (ER) defined in dB as:

$$\mathrm{CR} = 10\log\frac{\bar{P}^{1}_{\mathrm{tran}}}{\bar{P}^{0}_{\mathrm{refl}}}, \tag{18}$$

where $\bar{P}^{1}_{\mathrm{tran}}$ is the mean value of peak power of '1' at the transmission port and $\bar{P}^{0}_{\mathrm{refl}}$ the mean value of peak power of '0' at the reflection port,

$$\mathrm{AM} = 10\log\frac{P^{1}_{\max}}{P^{1}_{\min}}, \tag{19}$$

where $P^{1}_{\max}$ is the maximum value of peak power of '1' and $P^{1}_{\min}$ the minimum value of peak power of '1' at the transmission port and

$$\mathrm{ER} = 10\log\frac{P^{1}_{\min}}{P^{0}_{\max}}, \tag{20}$$

where $P^{1}_{\min}$ is the minimum value of peak power of '1' and $P^{0}_{\max}$ the maximum value of peak power of

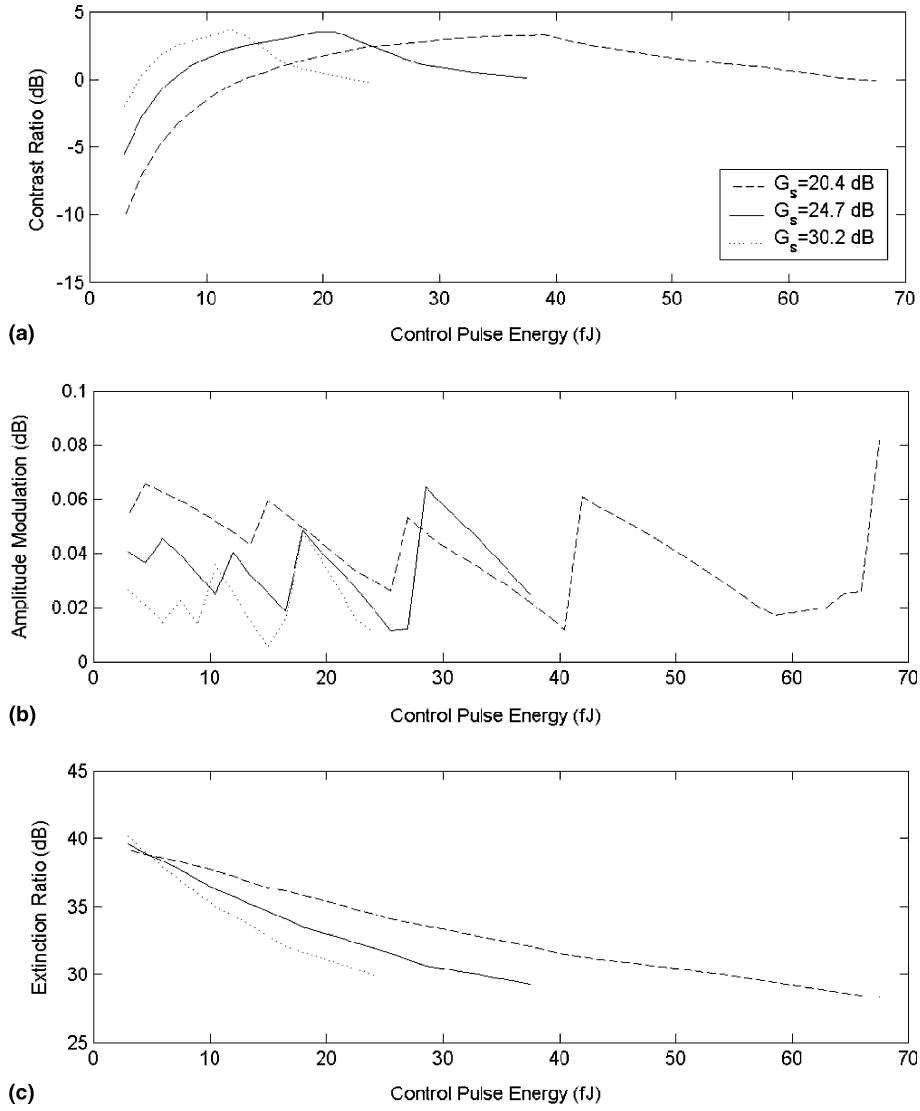

Fig. 3. Calculated metrics at 10 Gb/s for medium SOA saturation, (a) contrast ratio, (b) amplitude modulation and (c) extinction ratio.

'0' at the transmission port. For optimum gate performance, the contrast ratio must be as high as possible so that the largest fraction of the incoming clock signal exits at the transmission and not at the reflection port, the amplitude modulation as low as possible so that the output '1' have the same level (i.e. no pattern effect) and the extinction ratio as high as possible so that the '1' can be clearly distinguished from the '0'.

Initially, the degree of the SOAs saturation required to obtain the maximum contrast ratio or equivalently a differential phase shift of π radians, was investigated at 10 Gb/s in terms of the control and clock pulses energy, requiring from (17) that $\frac{G_1(t)}{G_2(t)} = 0.36$. For this purpose, three values of the clock energy inserted in the SOAs, namely 0.2, 3 and 40 fJ, were selected to correspond to low, medium and high (deep) saturation, respectively, depending on the degree of the small signal gain reduction. The control pulse energy was scanned to find the range over which the contrast ratio is positive so as to assure optimum switching. From

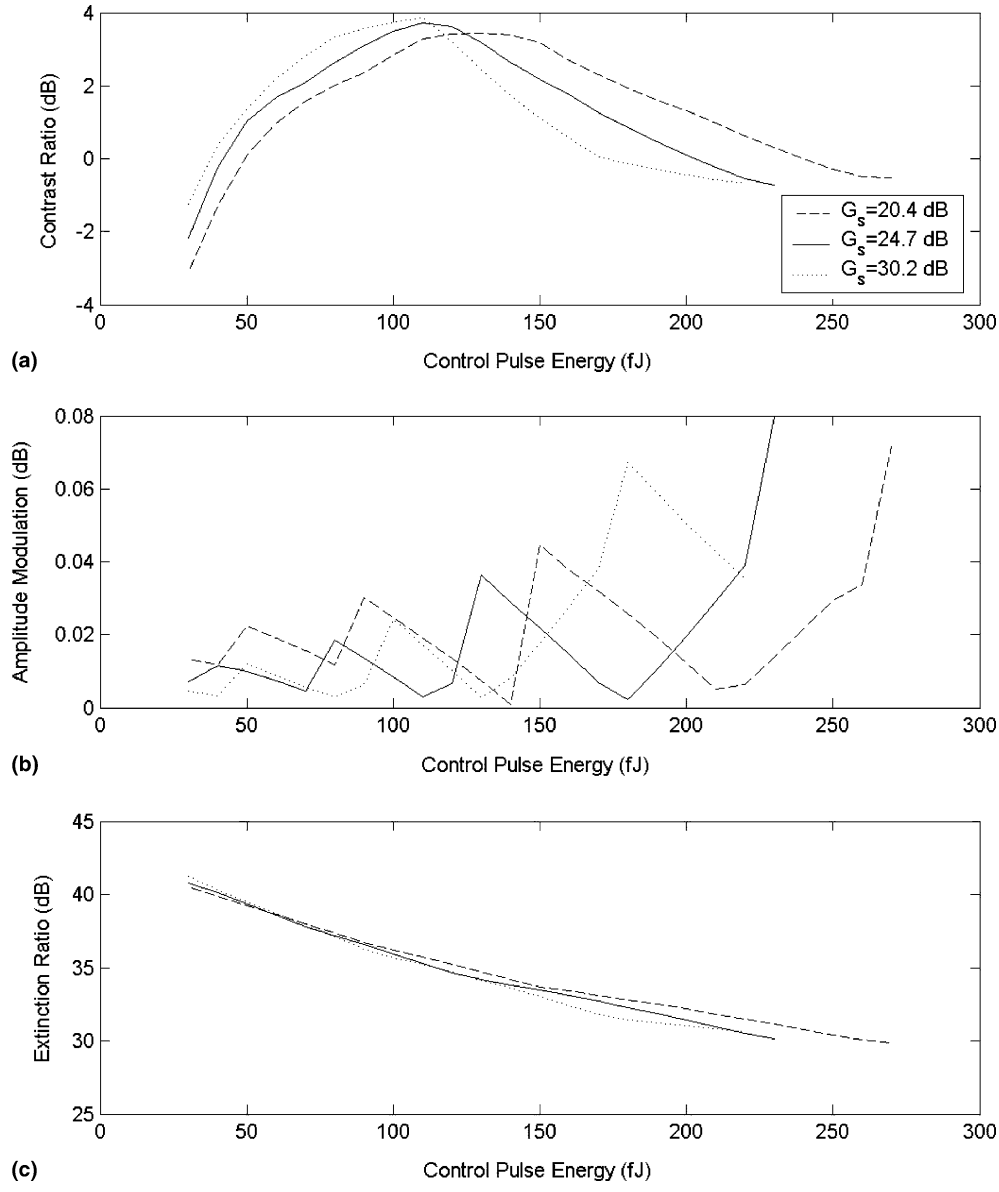

Fig. 4. Calculated metrics at 10 Gb/s for deep SOA saturation, (a) contrast ratio, (b) amplitude modulation and (c) extinction ratio.

the three sets of results that are depicted in Figs. 2–4, respectively, it was observed that this range increases with the increase of the degree of saturation and becomes wider when both SOAs are heavily saturated. However, there is an upper limit where the curve of the contrast ratio variation versus the control energy stops and which when it is exceeded, the switched-out pulses become severely distorted because more than one local power maxima occur during one bit period, as shown in Fig. 5. This is due to the asymmetric gain variation at the pulse leading and trailing edge and the significant increase of the differential phase shift over π radians, as it will be explained in more detail in the next section. The permissible control energy range varies inversely with the small signal

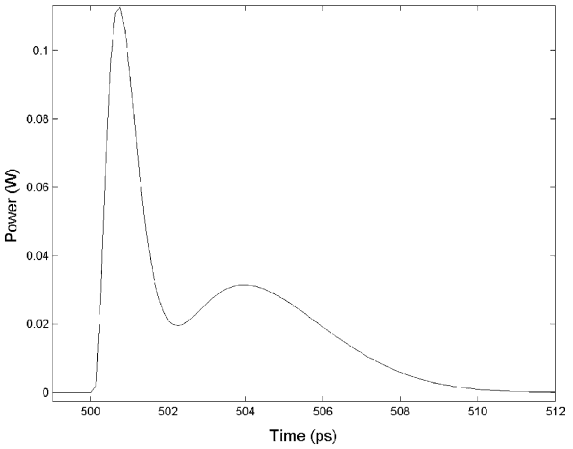

Fig. 5. Distorted output clock pulse at the transmission port.

gain, i.e. higher small signal gain values result in smaller energy ranges, but as the degree of saturation increases from the low to the heavy regime, this dependence becomes less intense. The increase of the saturation degree results also in the reduction of the ratio of the control and clock energies, which become comparable. Having defined the range of the control energy, we checked then the amplitude modulation and the extinction ratio. From Figs. 2–4(b) and (c), it is observed that the highest value of the former does not exceed 0.08 dB and the lowest value of the latter is always over 30 dB. These values are achieved independently of the degree of saturation and the values of the small signal gain, essentially implying that these two metrics do not impose limitations on the operation of the gate at 10 Gb/s, which is constant and predictable. Using SOAs with small gain of approximately 30 dB, two different data patterns shown in Fig. 6(a) and (b) with control energies, obtained from Fig. 4(a), 105 and 110 fJ, respectively, and clock energy 40 fJ, i.e. so that the SOAs are in the heavy saturation regime, the output logic signals of the XOR operation at the transmission and reflection port of the MZI are simulated and illustrated in Fig. 6(c) and (d), respectively. Fig. 6(c) shows correct XOR operation bit by bit, i.e. a '0' is produced if the bits of the patterns are identical and a '1' if they differ, without any pattern effect on the switched-out pulses. However, the output pulse stream at the reflection port does not correspond to the complement of the XOR result at the transmission port due to the SOAs different gain saturation. The physical mechanism behind this effect is the intense control pulses that deplete the SOAs carriers causing a change of their gain and refractive index and as a consequence a phase change between the upper and lower MZI arm clock pulses. Although the phase change is necessary to achieve switching when the clock pulses recombine back to the 3 dB coupler, the gain change is undesirable because it deteriorates the output contrast ratio and distorts the switching data [27]. The maximum possible switching can be achieved only if the relative magnitude of phase nonlinearities is maximized over the gain nonlinearities. However, this goal cannot be easily achieved in the case of semiconductor nonlinearities where the gain and phase difference are related via the enhancement factor according to (17). The differential gain is thus inevitable and an inherent characteristic of such type SOA-based interferometric configurations. As a result, full destructive interference is impossible and a part of the clock signal leaks at the reflection port. More specifically, at the time intervals in which a '0' is expected at this port, i.e. when the control patterns differ, the gains experienced by the clock pulses in the two arms of the MZI also differ and as a consequence a significant power level that equals at least $1/4P_{\mathrm{in}}(t)\{G_1(t)+G_2(t)-2\sqrt{G_1(t)G_2(t)}\}$ appears at the reflection port, where $P_{\mathrm{in}}(t)$ is the clock input power. Similarly, at the time intervals where a '1' is expected, the SOAs gains can be either high or low, depending on whether both controls are '0' or '1', respectively. As a consequence, the clock pulses are unevenly amplified and their power at the reflection port is not the same.

In order to assess whether the SOAs exhibiting the properties of Table 1 are adequate to extend the Boolean XOR operation at 40 Gb/s or not, simulation results were obtained at this bit rate for the same metrics as at 10 Gb/s, shown in Figs. 7–9. The direct comparison of the contrast ratio curve of Figs. 2–4(a) at 10 Gb/s with the corresponding ones 7(a), 8(a) and 9(a) at 40 Gb/s reveals that the behaviour of the gate concerning the permissible control energy range is essentially the same. The amplitude modulation and the extinction ratio, on

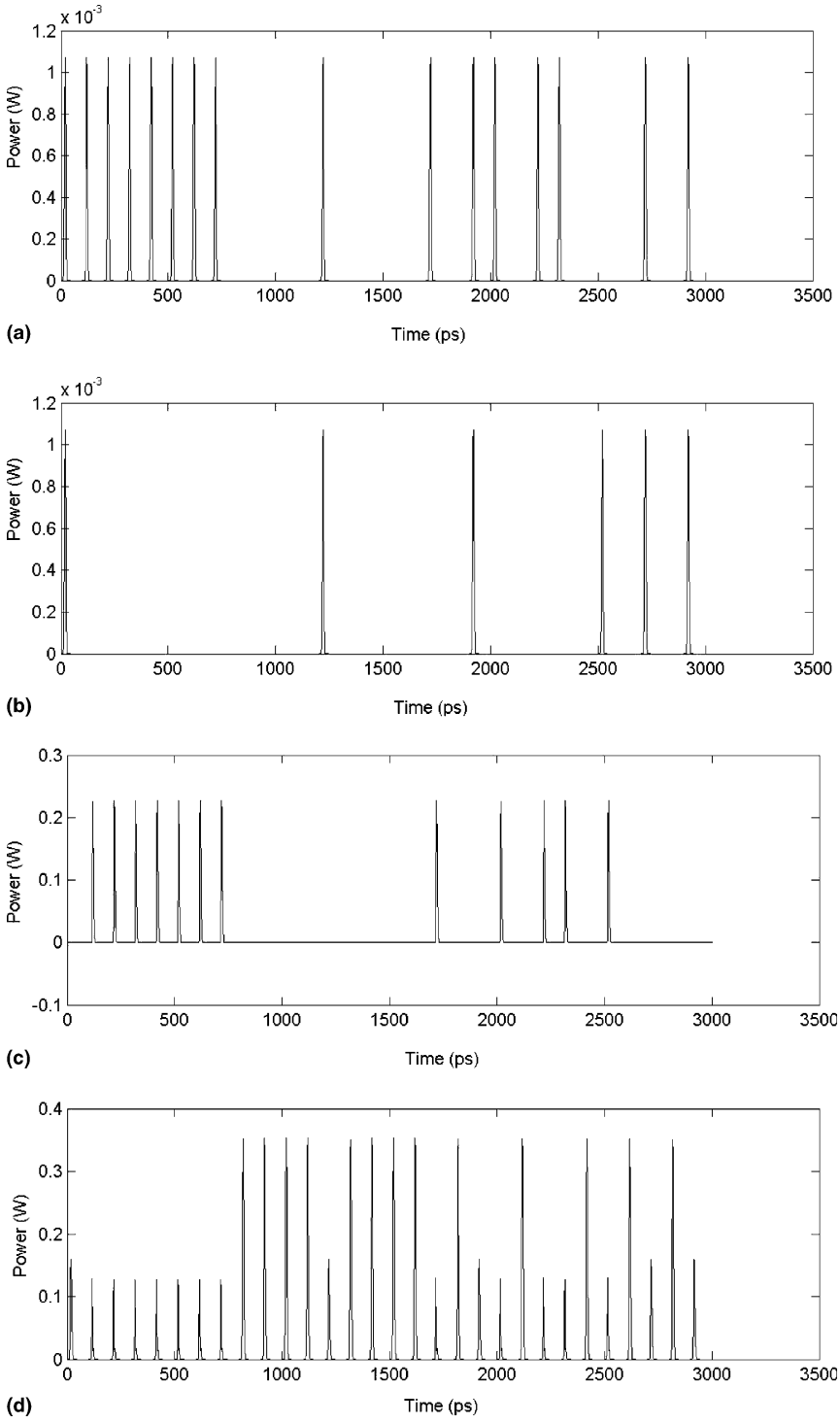

Fig. 6. Simulation results of the XOR operation at 10 Gb/s, (a) control input A, (b) control input B, (c) XOR output at transmission port and (d) XOR output at reflection port.

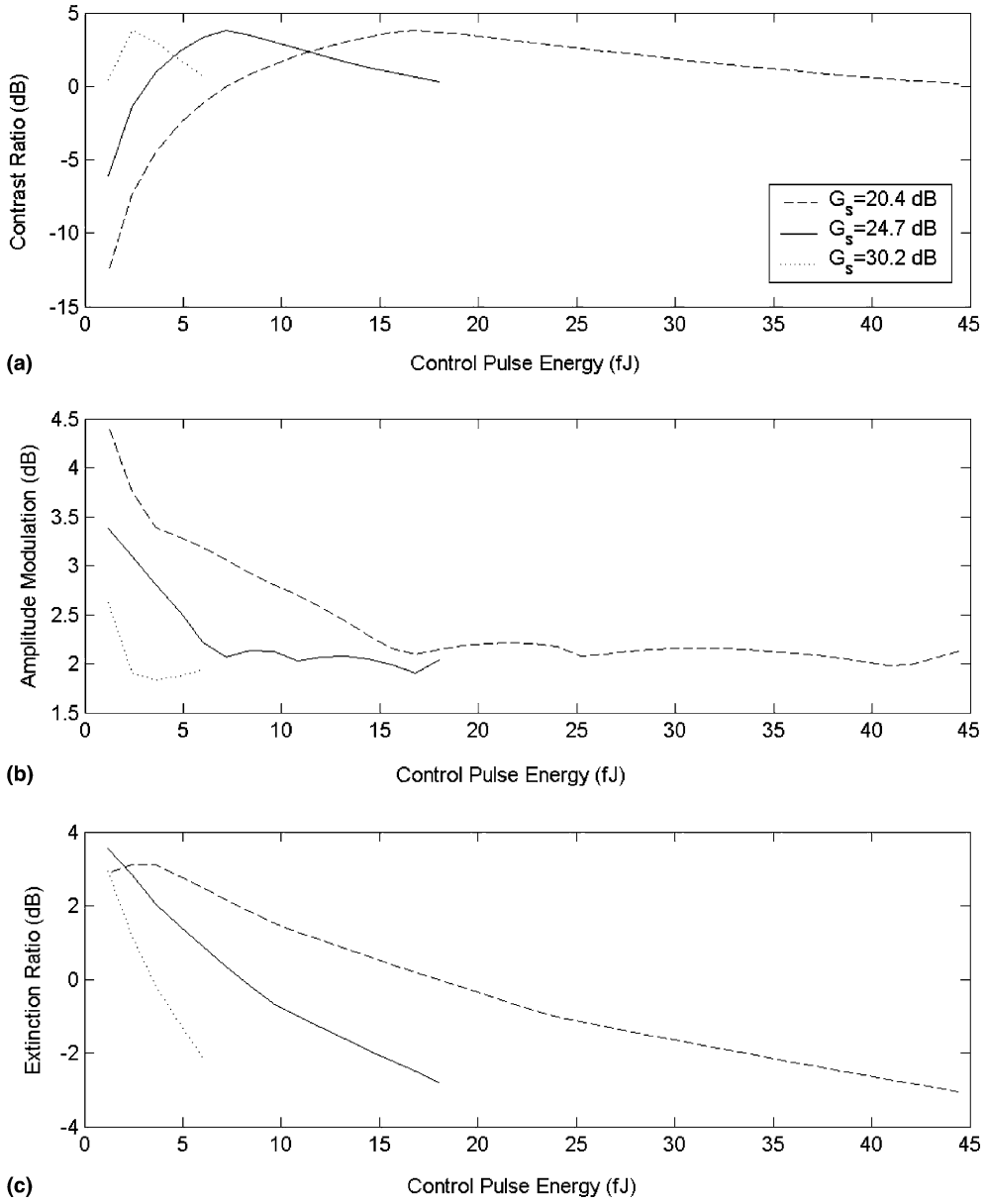

Fig. 7. Calculated metrics at 40 Gb/s for low SOA saturation, (a) contrast ratio, (b) amplitude modulation and (c) extinction ratio.

the contrary, change significantly affecting the gate's performance in a negative way and impeding operation at 40 Gb/s. The increase of the small signal gain improves the amplitude modulation but not the extinction ratio. A significant improvement of the gate's performance in terms of the amplitude modulation is observed under heavy saturation, since the more the gain is saturated, the less is its value varied versus the power and the pattern of the control pulse stream. As a consequence, the clock pulses suffer almost the same gain and their amplification is uniform. Unfortunately, even though the extinction ratio is also improved for deep saturation, its value is still small

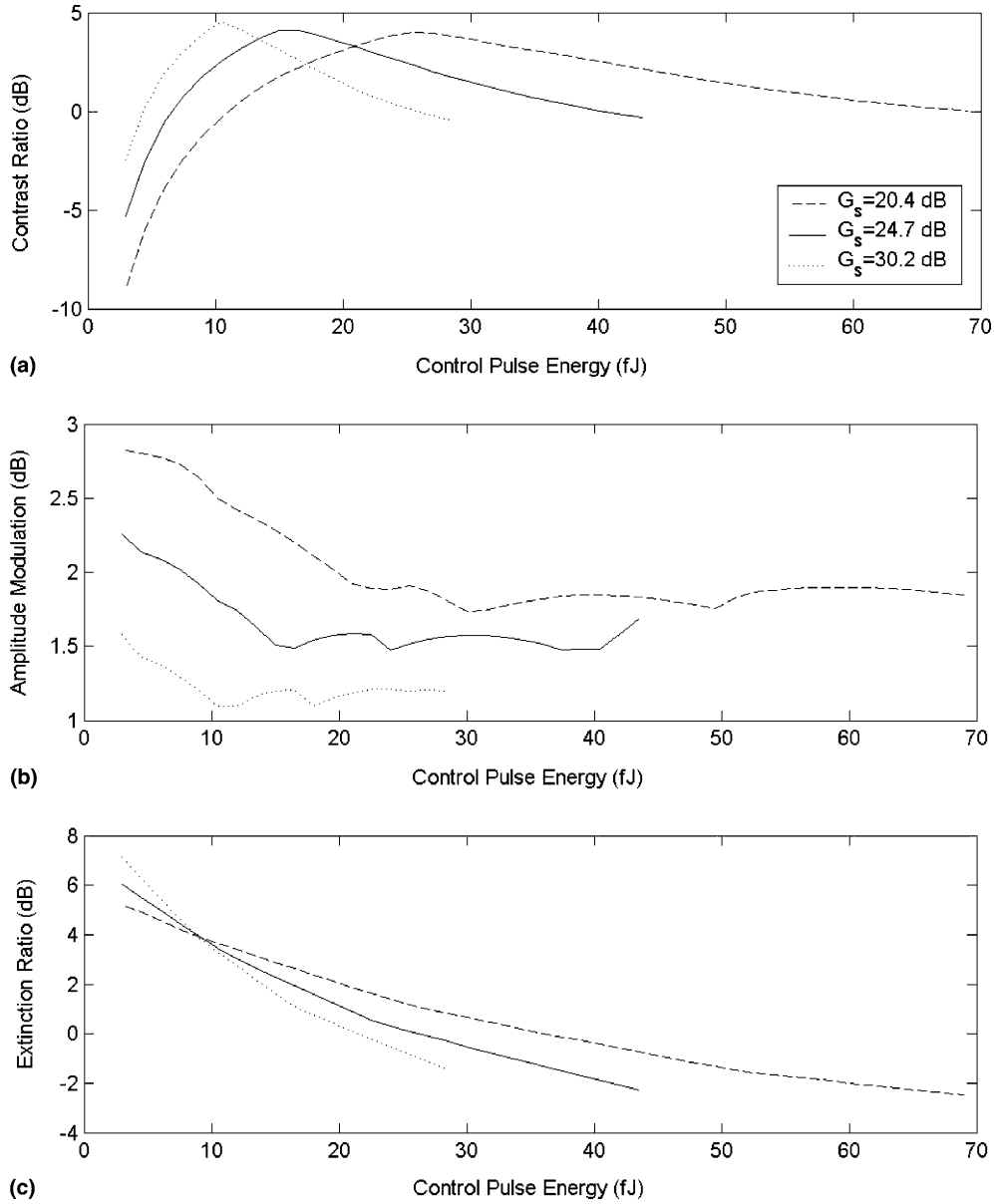

Fig. 8. Calculated metrics at 40 Gb/s for medium SOA saturation, (a) contrast ratio, (b) amplitude modulation and (c) extinction ratio.

enough for adequate 40 Gb/s operation using the specific SOA devices. Using the same control data patterns as at 10 Gb/s, small signal gain of approximately 30 dB and control and clock energies 90 and 80 fJ, respectively, that correspond to the heavily saturated SOA, the XOR results at the transmission and reflection ports are shown in Fig. 10(c) and (d), respectively, which are governed by a strong bit pattern dependence or equivalently a small value of the extinction ratio. This is due to the long SOA carrier lifetime that exceeds by far the bit period, which at 40 Gb/s is 25 ps, and determines the temporal evolution of the gains and phases of the clock pulses at the output of the

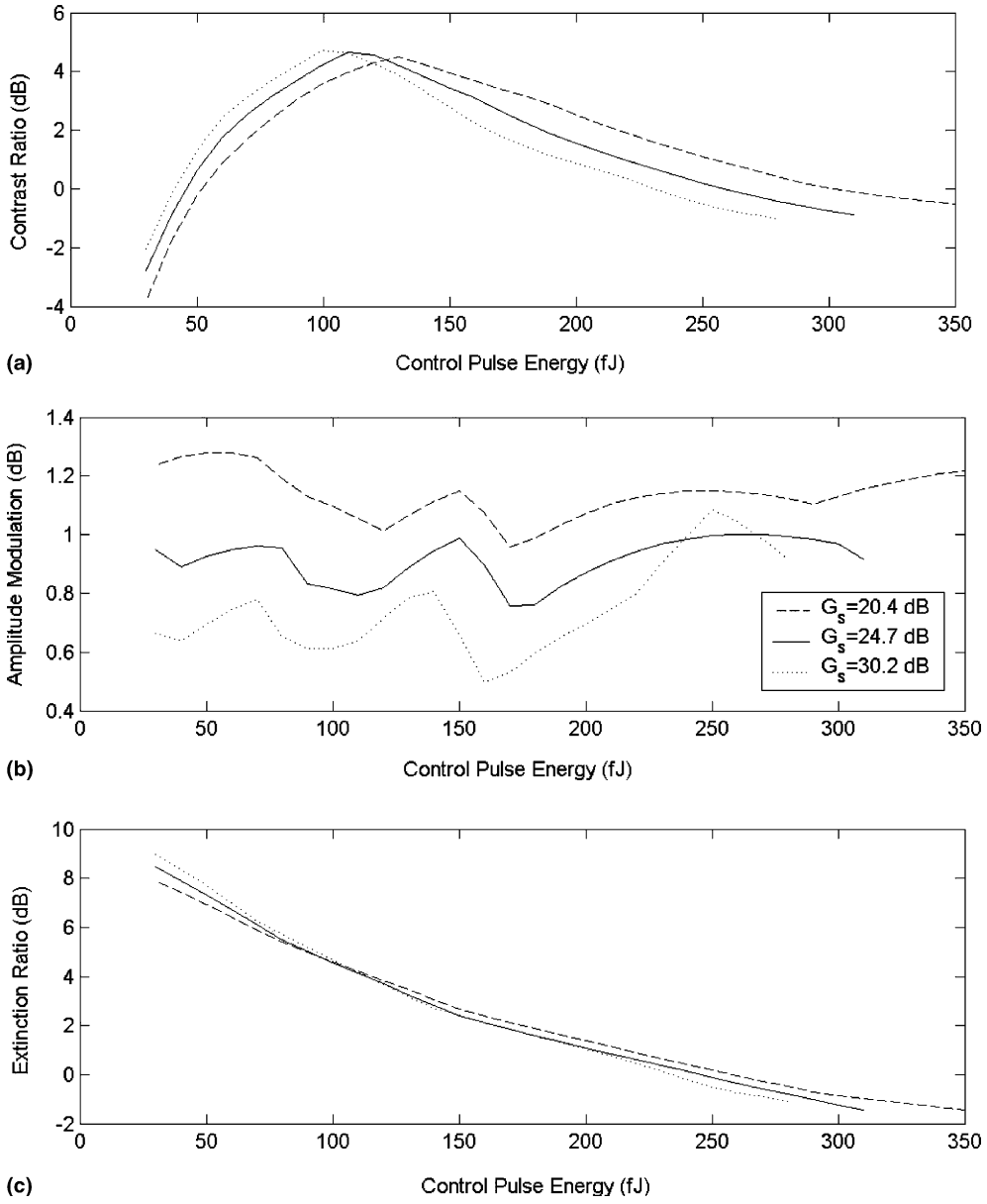

Fig. 9. Calculated metrics at 40 Gb/s for deep SOA saturation, (a) contrast ratio, (b) amplitude modulation and (c) extinction ratio.

SOAs in the upper and lower MZI arms, illustrated in Figs. 11 and 12, respectively. From these figures it can be observed that the gain drops rapidly during the '1' bit period which leads to an abrupt phase change of the clock, whilst the '0' bit period allows the gain to recover. Moreover, continuous '0' bits help the gain to rise further whilst continuous '1' bits impede the gain to recover fully. The result is that the gain and thus the amplitude of a specific bit depends on the preceding bits, leading to amplitude distortion at the output. This effect is more intense at the time intervals where there is a change from '1' to '0' and vice versa, since a '1' saturates strongly the SOA

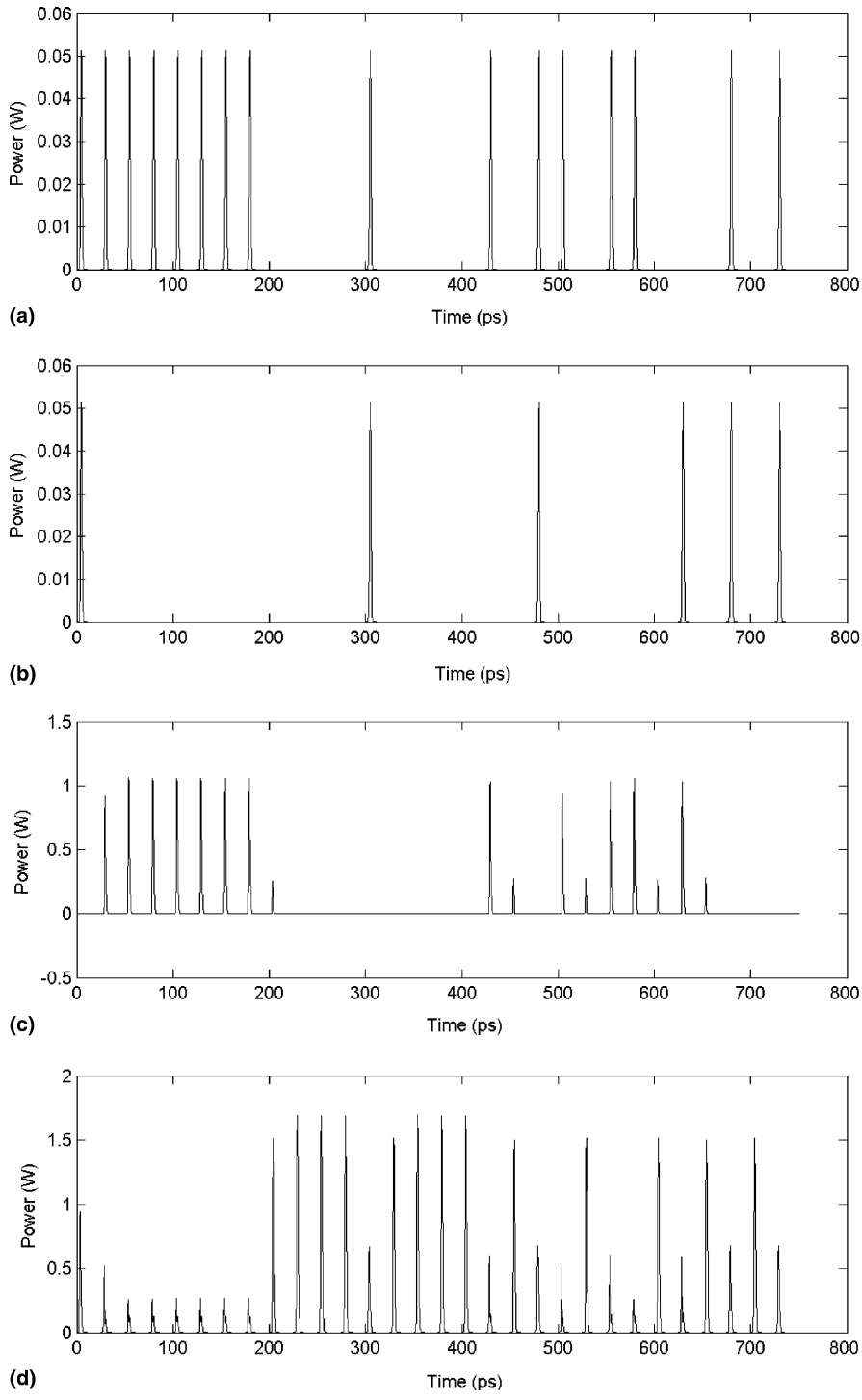

Fig. 10. Simulation results of the XOR operation at 40 Gb/s, (a) control input A, (b) control input B, (c) XOR output at transmission port and (d) XOR output at reflection port.

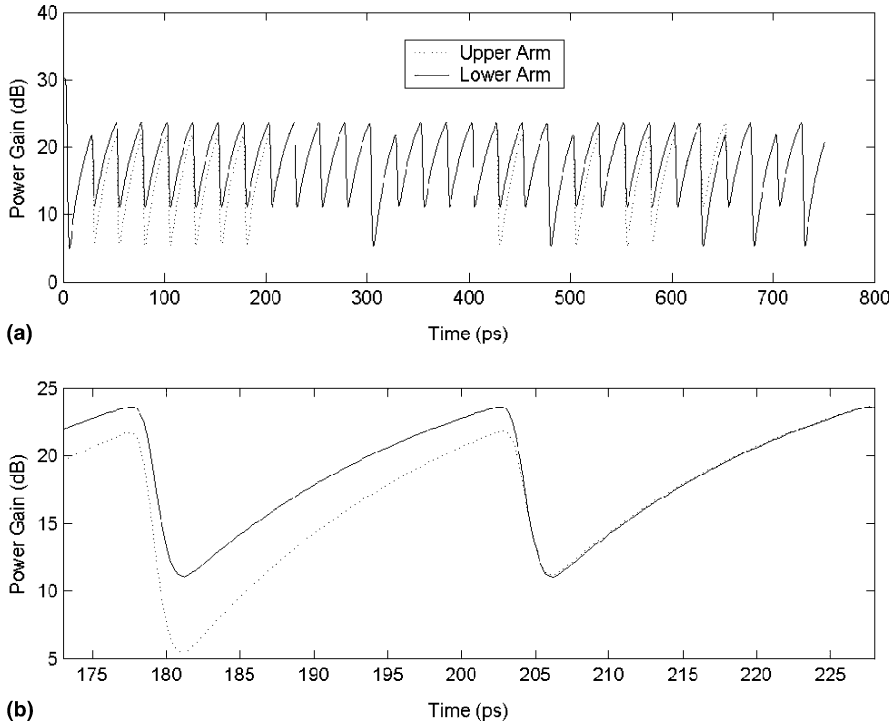

Fig. 11. Temporal evolution of the SOA gains in the upper and lower MZI arms (a) and a detail of the seventh and eighth pulse (b).

and the '0' that follows leaves enough time for gain recovery so that the next '1' exhibits a different gain and phase change than the previous '1'. Despite thus the fact that the XOR truth table is realized correctly in Fig. 10(c) and (d), the strong pattern dependence ascribed to the advent of '1' and '0' does not permit the extinction ratio to exceed 10 dB.

The performance of the SOA-MZI XOR gate at 40 Gb/s can be significantly improved and become similar to that at 10 Gb/s using shorter FWHM pulses provided by laser sources [28] in combination with faster recovery times that can be achieved using either strong saturating holding beams to drive bulk or quantum-well SOAs [29,30] or the novel technology of quantum-dot SOAs. This technology has attracted considerable interest during the recent years due to several characteristics that offer significant performance improvement over conventional bulk and quantum-well amplifiers. Among these are the very wide gain bandwidths, inhomogeneous broadened gain spectra, high saturation powers, pattern-effect-free operation and two to three orders faster response speed that can enable the achievement of ultrahigh switching speeds in various all-optical signal processing tasks [31]. However, their linewidth enhancement factor is smaller compared to conventional bulk SOAs [32], making difficult the achievement of the phase shifts required for switching. Further research is required thus in order to assess whether this technology can be exploited in all-optical switching modules that are based in interferometric configurations.

4. Distortion of propagating pulses

In this section we discuss the issue of the distortion of the clock pulses as they propagate through the all-optical gate. The occurrence of this phenomenon is attributed to the temporal variation of the SOAs gain and the differential phase shift during a bit period that results in different gains and phase shifts exhibited between the leading and trailing edge of the same pulse. Since the trans-

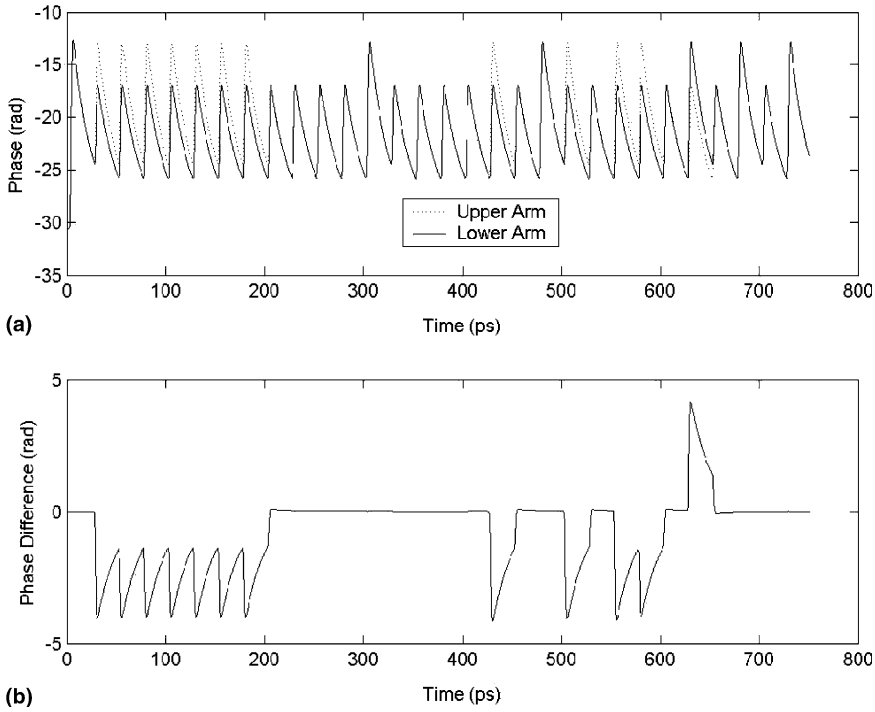

Fig. 12. Temporal evolution of the phase (a) and differential phase shift (b) of the clock pulses at the SOA outputs in the upper and lower MZI arms.

mission function depends, from (15), on the gain and phase shift, which in turn depend on time, the output pulse power follows the time variation of these two parameters and becomes thus distorted.

In the following, we focus only on the 10 Gb/s rate, since the results at 40 Gb/s are similar, for the three cases of SOAs saturation discussed in the previous section. The energy of the control pulses is chosen to correspond to the peak value of the contrast ratio curve of Figs. 2,3,4(a). The low, medium and high saturation regimes are expressed thus by the pair of clock and control energies (0.2, 2.4 fJ), (3, 7.5 fJ) and (40, 70 fJ), in Figs. 13–15, respectively. For each saturation regime, four diagrams (a), (b), (c) and (d) are presented. The first is the power of the fifth incoming clock pulse and so the time on the horizontal axis spans from 400 to 500 ps. The pulse peak occurs at 420 ps. The second and third diagram depicts the temporal variation of the power gain and differential phase shift, respectively. Finally, the fourth diagram illustrates the corresponding output clock pulse at the transmission port of the MZI. The two control pulse trains are the same as in Fig. 6(a) and (b).

The distortion consists in the suppression of the pulse leading edge and the shift of its peak power to the left of the time axis, i.e. towards shorter time values. As it can be seen from the power gain curve in the two arms of the MZI (second diagram), the pulse leading edge exhibits a high gain, because the two SOAs have not become yet saturated. As a direct consequence, this part of the pulse is highly amplified but also suppressed, because the corresponding differential phase shift is zero (from (17), since $G_1 = G_2$) and so, according to (15), the output power is also zero (again since $G_1 = G_2$). The higher the saturation degree, the faster the gain is saturated and the absolute differential phase shift is increased. In other words, under heavy saturation the suppression of the leading edge is smaller, as it can be clearly seen from the comparison of Figs. 13–15.

The output pulse becomes maximum when, from (15), the differential phase shift is $\pm\pi$ radians.

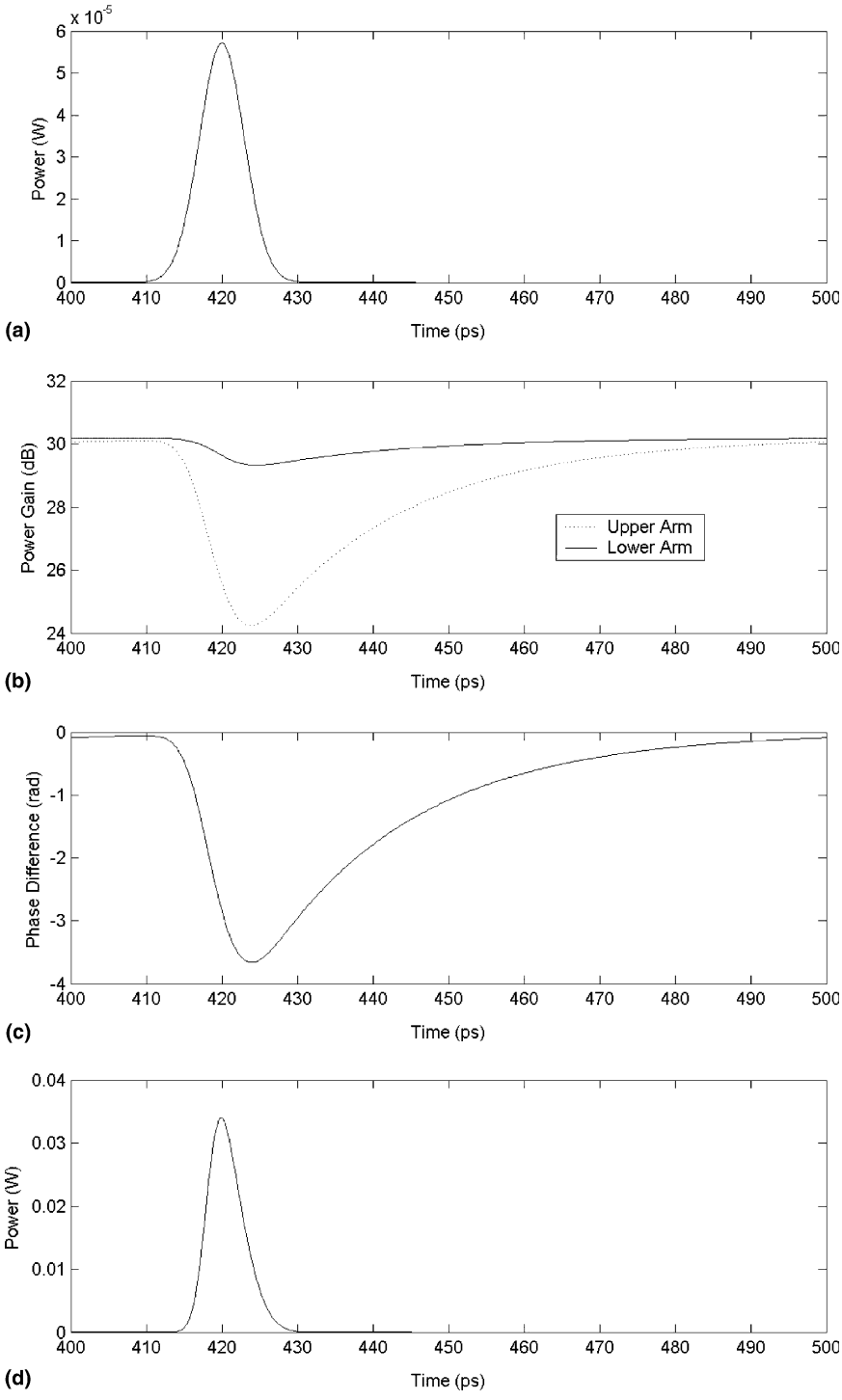

Fig. 13. Fifth input clock pulse (a) and temporal evolution of its gain (b) and differential phase shift (c) that result in strong distortion at the MZI output (d), for low SOA saturation.

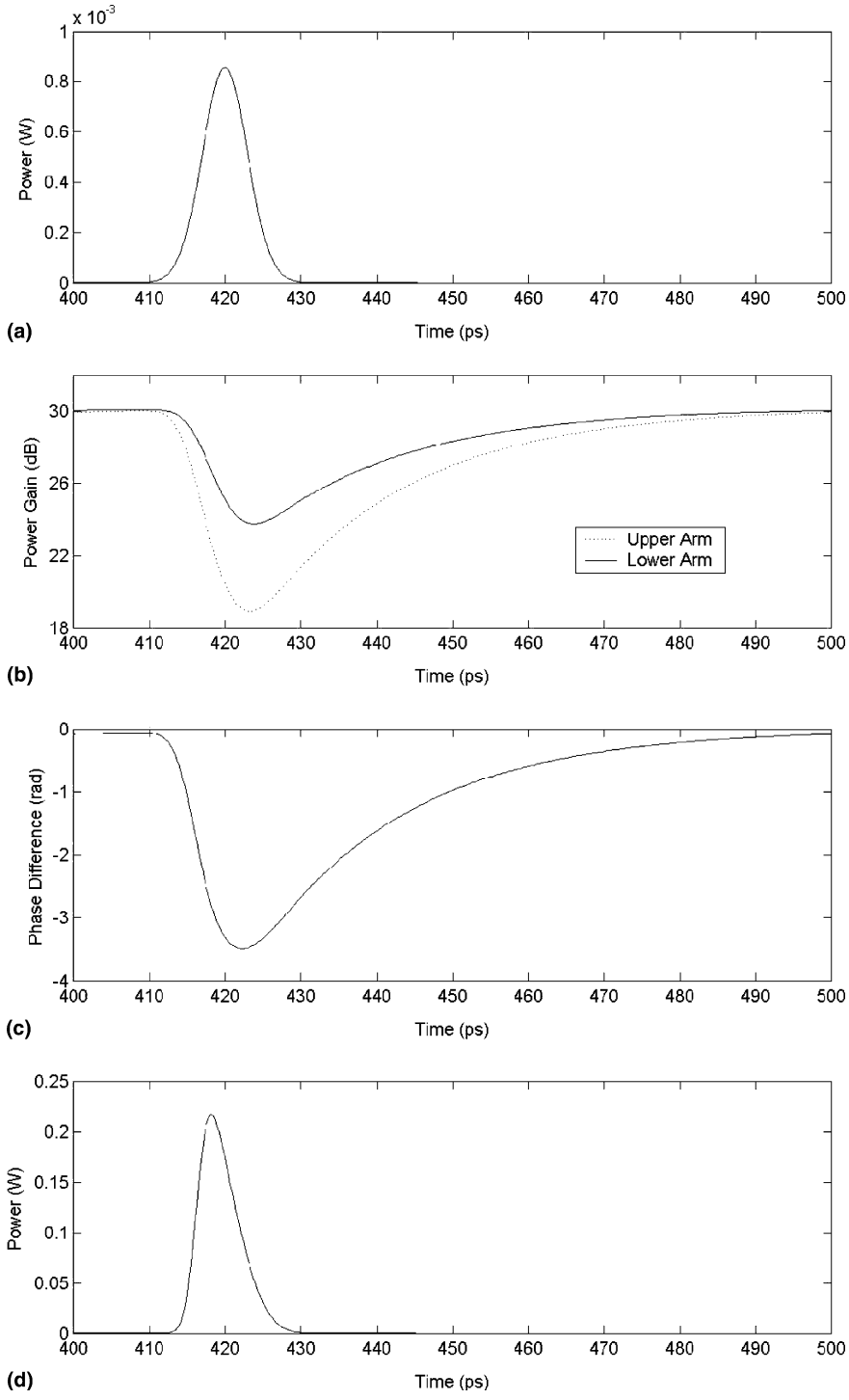

Fig. 14. Fifth input clock pulse (a) and temporal evolution of its gain (b) and differential phase shift (c) that result in strong distortion at the MZI output (d), for medium SOA saturation.

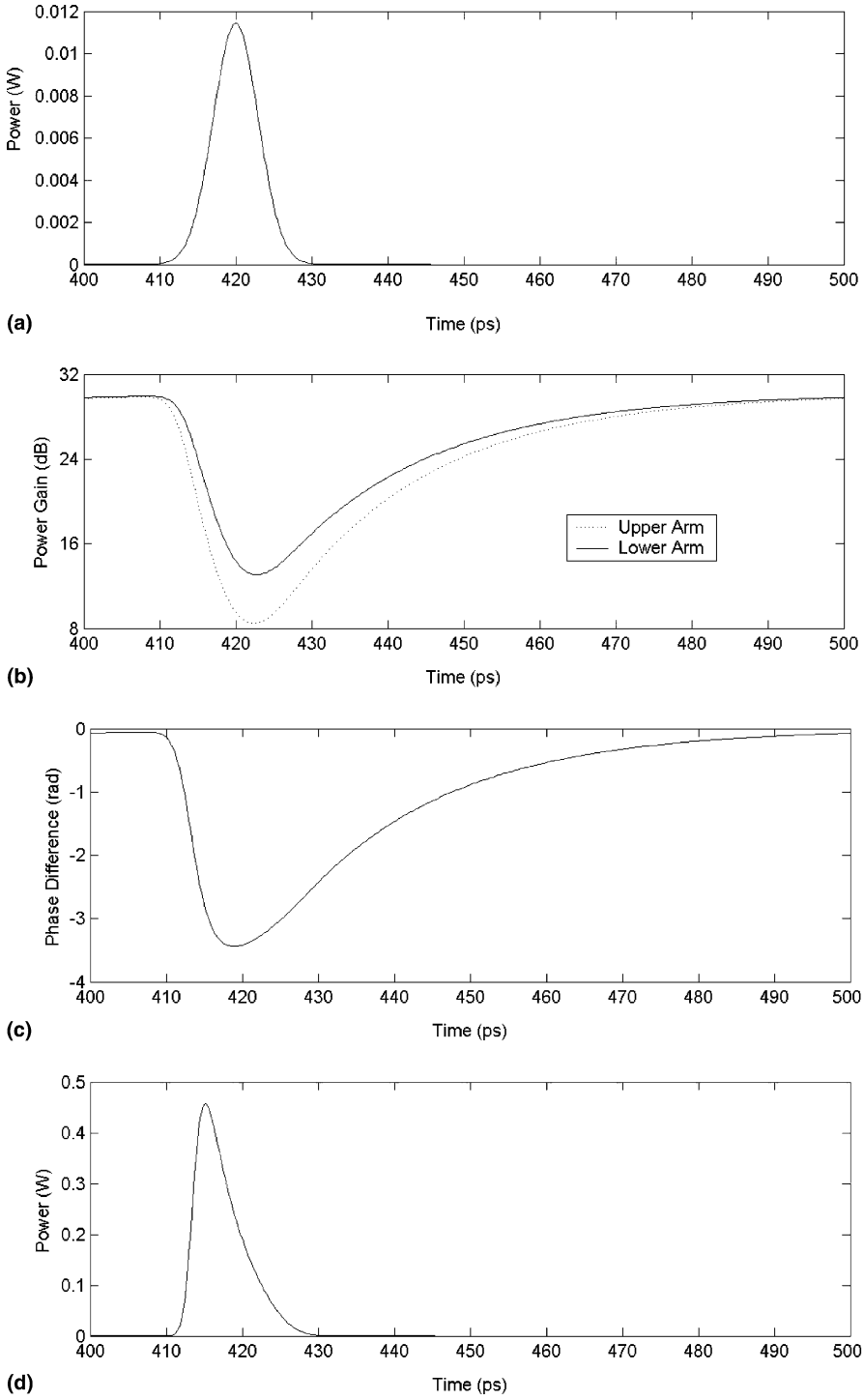

Fig. 15. Fifth input clock pulse (a) and temporal evolution of its gain (b) and differential phase shift (c) that result in strong distortion at the MZI output (d), for deep SOA saturation.

Since this does not happen exactly at 420 ps, the peak power is temporally shifted. As the saturation degree increases, the differential phase shift approaches faster the value $\pm\pi$ due to the faster saturation. This is the reason for which the peak of the output pulse in Fig. 15(d) has been much more shifted than in the case of Figs. 13(d) and 14(d).

From the moment that the output pulse power is maximized until the time of 430 ps that it becomes practically zero, the differential phase shift is near the area of $\pm\pi$. Furthermore, the gain variation during the same interval is not so intense. As a consequence, the variation of the phases as well as of the gains is significantly smaller than at the first 8 ps of the pulse and thus the trailing edge is less suppressed than the leading edge.

In case that only the gain was varied in time, the power at the two pulse edges would be amplified much more than at the pulse center. If, on the contrary, the gain was constant and only the differential phase shift was time varying, the middle part of the pulse would be mainly switched at the transmission port and its edges less. The gain and phase variations compensate thus each other resulting in a smaller pulse distortion than that it would occur if only one of the time variation was present.

It must be noted that the distortion of the pulses is much more severe when the control pulse energy has overcome the upper limit discussed in the previous section. The reason for this is that the maximum absolute differential phase shift deviates significantly from the ideal $\pm\pi$ radians and for very high energy values it can surpass by far 2π or even 3π. This can be understood assuming, for example, that the maximum absolute differential phase shift is 2π. According to the time variation curve, the differential phase shift starts from the zero value where the output power at the switching port is zero, passes from the $\pm\pi$ area where the output power is maximum and as it leaves it the power starts to decrease. Due to the 2π value, however, the phase reaches a second maximum and as a result, the output pulse has two local maxima, as shown in Fig. 5. It must be noted that these results are in accordance with the ones obtained from the characterization of the phase dynamics of the same, single 1500 μm SOA device used in the simulation [21]. It is thus the first time that they are verified and extended for the case of a SOA-MZI XOR gate.

5. Conclusion

In conclusion, we have numerically simulated the SOA-MZI XOR gate at 10 and 40 Gb/s in order to investigate the suitable operating conditions and derive simple design rules for the improvement of its performance in terms of the metrics that define the quality of switching. The obtained results indicate that at both rates the SOAs must be preferably operated under heavy saturation since then, the range of the energy of the control pulses is wider and the behaviour of the gate is constant and almost independent of the small signal gain. At the same time, the control pulse energy must not exceed an upper limit over which the switched-out pulses become severely distorted. Provided that these operational criteria are satisfied, the gate can be realized with high performance at 10 Gb/s. However, the extension of the operation of the gate to 40 Gb/s using the same SOA modules as at 10 Gb/s is limited by the SOA gain recovery time that results in strong pattern dependence and performance degradation. As a consequence, major improvements in the performance of conventional bulk SOAs are required, which can be achieved by deploying successfully tested gain recovery reduction techniques. An alternative solution in order to meet the higher speed requirements is to exploit the novel technology of quantum-dot SOAs and take advantage of its attractive operational features and ultrafast gain dynamics to perform ultra-high speed all-optical signal processing. This numerical simulation may be expanded to analyze other more complex all-optical circuits in which the XOR gate is the basic building block and cannot be sufficiently simulated by the commercially available photonic software tools. The obtained results will significantly contribute to the deeper understanding and more efficient exploitation of the SOA-based all-optical switches.

References

[1] H. Avramopoulos, IEEE LEOS Summer Top. ME2 (2002).
[2] K.E. Stubkjaer, IEEE J. Select. Top. Quantum Electron. 6 (2000) 1428.

[3] H.J.S Dorren, G.D. Khoe, D. Lenstra, Opt. Commun. 205 (2002) 247.
[4] C. Schubert, J. Berger, U. Feiste, R. Ludwig, C. Schmidt, H.G. Weber, IEEE Photon. Technol. Lett. 13 (2001) 1200.
[5] K. Tajima, S. Nakamura, Y. Ueno, Opt. Quantum Electron. 33 (2001) 875.
[6] M. Dülk, S. Fischer, M. Bitter, M. Caraccia, W. Vogt, E. Gini, H. Melchior, W. Hunziker, A. Buxens, H.N. Poulsen, A.T. Clausen, Opt. Quantum Electron. 33 (2001) 899.
[7] Y. Ueno, S. Nakamura, K. Tajima, IEEE Photon. Technol. Lett. 13 (2001) 469.
[8] M.L. Nielsen, M. Nord, M.N. Petersen, B. Dagens, A. Labrousse, R. Brenot, B. Martin, S. Squedin, M. Renaud, Electron. Lett. 39 (2003) 385.
[9] S. Fischer, M. Bitter, M. Caraccia, M. Dulk, E. Gamper, W. Vogt, E. Gini, H. Melchior, W. Hunziker, Opt. Lett. 26 (2001) 626.
[10] M.T. Hill, H. de Waardt, G.D. Khoe, H.J.S. Dorren, Microwave Opt. Technol. Lett. 31 (2001) 411.
[11] J.M. Martinez, F. Ramos, J. Marti, J. Herrera, R. Llorente, ECOC P4.8 (2002).
[12] S. Lee, J. Park, K. Lee, D. Eom, S. Lee, J.H. Kim, Jpn. J. Appl. Phys. 2 (41) (2002) L1155.
[13] H. Chen, G. Zhu, Q. Wang, J. Jaques, J. Leuthold, A.B. Piccirilli, N.K. Dutta, Electron. Lett. 38 (2002) 1271.
[14] T. Fjelde, D. Wolfson, A. Kloch, B. Dagens, A. Coquelin, I. Guillemot, F. Gaborit, F. Poingt, M. Renaud, Electron. Lett. 36 (2000) 1863.
[15] R.P. Webb, R.J. Manning, G.D. Maxwell, A.J. Poustie, Electron. Lett. 39 (2003) 79.
[16] S. Bischoff, A. Buxens, St. Fischer, M. Dülk, A.T. Clausen, H.N. Poulsen, J. Mørk, Opt. Quantum Electron. 33 (2001) 907.
[17] R.P. Schreieck, M.H. Kwakernaak, H. Jäckel, H. Melchior, IEEE J. Quantum Electron. 38 (2002) 1053.
[18] Y. Ueno, S. Nakamura, K. Tajima, J. Opt. Soc. Am. B 19 (2002) 2573.
[19] J.M. Tang, K.A. Shore, IEEE J. Quantum Electron. 34 (1998) 1263.
[20] R. Gutiérrez-Castrejón, L. Schares, L. Occhi, G. Guekos, IEEE J. Quantum Electron. 36 (2000) 1476.
[21] L. Schares, C. Schubert, C. Schmidt, H.G. Weber, L. Occhi, G. Guekos, IEEE J. Quantum Electron. 39 (2003) 1394.
[22] A. Mecozzi, J. Mørk, J. Opt. Soc. Am. B 14 (1997) 761.
[23] J.M. Tang, K.A. Shore, IEEE J. Quantum Electron. 35 (1999) 1704.
[24] J. Mørk, A. Mecozzi, IEEE J. Quantum Electron. 33 (1997) 545.
[25] G.P. Agrawal, N.A. Olsson, IEEE J. Quantum Electron. 25 (1989) 2297.
[26] K.I. Kang, T.G. Chang, I. Glesk, P.R. Prucnal, Appl. Opt. 35 (1996) 417.
[27] R.J. Manning, A.E. Kelly, A.J. Poustie, K.J. Blow, Electron. Lett. 34 (1998) 916.
[28] C.J.S. de Matos, D.A. Chestnut, J.R. Taylor, Appl. Phys. Lett. 81 (2002) 2932.
[29] M.T. Hill, E. Tangdiongga, H. de Waardt, G.D. Khoe, H.J.S. Dorren, Opt. Lett. 27 (2002) 1625.
[30] R.J. Manning, G. Sherlock, Electron. Lett. 31 (1995) 307.
[31] M. Sugawara, T. Akiyama, N. Hatori, Y. Nakata, H. Ebe, H. Ishikawa, Meas. Sci. Technol. 13 (2002) 1683.
[32] M.V. Maximov, L.V. Asryan, Y.M. Shernyakov, A.F. Tsatsul'nikov, I.N. Kaiander, V.V. Nikolaev, A.R. Kovsh, S.S. Mikhrin, V.M. Ustinov, A.E. Zhukov, Z.I. Alferov, N.N. Ledenstou, D. Bimberg, IEEE J. Quantum Electron. 37 (2001) 676.